Direct detection of pulsations of the Cepheid star ζ Gem and an independent calibration of the period–luminosity relation

B. F. Lane*, M. J. Kuchner*, A. F. Boden†, M. Creech-Eakman‡ & S. R. Kulkarni*

* *Palomar Observatory 105-24,* † *Infrared Processing and Analysis Center,*
‡ *Jet Propulsion Laboratory 171-113, California Institute of Technology, Pasadena*

Cepheids are a class of variable (pulsating) stars whose absolute luminosities are related in a simple manner to their pulsational periods. By measuring the period and using the 'period–luminosity' relationship, astronomers can use the observed visual brightness to determine the distance to the star. Because these stars are very luminous, they can be observed in other galaxies, and therefore can be used to help determine the expansion rate of the Universe[1] (the Hubble constant). Calibration of the period–luminosity relation is a necessary first step, but the small number of sufficiently nearby Cepheids has forced the use of a number of indirect means, with associated systematic uncertainties. Here we present a distance to the Cepheid ζ Geminorum, determined using a direct measurement (by an optical interferometer) of its changes in diameter as it pulsates. Within our uncertainty of 15 per cent, our distance is in agreement with previous indirect determinations. Planned improvements to the instrument will allow us to calibrate directly the period–luminosity relation to better than a few per cent.

The Baade–Wesselink (BW) method of determining distance to a pulsating star[2] has long been regarded as a promising approach to calibrating the Cepheid distance scale[3,4]. The essence of the BW method is to combine measurements of physical radius changes with measurements of angular diameter changes (the distance is their ratio). Although physical radius changes are easily determined from radial velocity measurements, obtaining angular diameter measurements of distant stars is more challenging. Lacking direct measurements of the angular diameters of Cepheids, astronomers have had to infer angular diameter from multicolour photometry, with the attendant potential penalty of systematic error. Long-baseline interferometry offers the possibility of directly measuring angular diameter changes of nearby Cepheids. However, whereas the mean angular diameters of a few Cepheids have been measured by several groups[5–7], the detection of angular diameter changes has been elusive.

The Cepheid variable ζ Geminorum (HD52973) is a bright ($m_V = 3.62$–4.18) galactic Cepheid with a 10.15-day pulsational period[8]. From previous work[9,10] ζ Gem was expected to have an angular diameter in the range 1.2–2.2 milliarcseconds (mas; 1 mas $= 4.85 \times 10^{-9}$ radians), resolvable by the Palomar Testbed Interferometer[11] (PTI). We observed ζ Gem in the H band (1.6 μm) over a two-week period; see Table 1 for a log of the observations. The system response was monitored and calibrated by interleaving observations of ζ Gem, a calibration star (HD49968) and a check star (HD48450). These two stars were chosen to have angular sizes and brightness similar to those of the target star and to be located in close angular proximity on the sky (≤10 degrees); see Table 2.

The primary observable measured by PTI is the amplitude (often called the visibility) of the Young's fringe pattern created by combining starlight collected from two 40-cm apertures separated by a 110-m interferometric baseline. These fringe visibilities are related in a simple manner to the apparent angular diameter of the observed star (Table 1). The calibration of the visibilities—an important step in interferometry—followed standard procedures discussed elsewhere[12,13]. Results are shown in Table 2 and displayed in Fig. 1. It is clear that the angular diameter of ζ Gem is undergoing changes while the angular diameter of the check star is constant; the magnitude of the diameter changes is about 10%, consistent with theoretical expectations. We searched for periodicity in the vicinity of 10 days and found a significant peak in the power spectrum at $P \approx 10.2$ days. Monte Carlo simulations show that the probability that this peak is due to noise is less than 0.2%.

For this work, we integrated a previously published radial velocity

Table 2 Relevant parameters of the calibrator and check star, including spectral type apparent H-band magnitude (m_H) and angular distance from ζ Gem

Star ID	Spectral type	m_H	θ_{UD} (mas)	θ_{LD} (mas)	Angular separation (degrees)
HD49968	K5III	2.44	1.78 ± 0.1	1.90 ± 0.1	4.1
HD48450	K4III	~2.4	1.98 ± 0.4	2.09 ± 0.4	9.5

The limb-darkened angular diameter (θ_{LD}) of HD49968 was based on recent spectrophotometry[20], while θ_{LD} for HD48450 was estimated by fitting a blackbody to archived broad-band photometry. The relation between θ_{UD} and θ_{LD} is given by the approximation[21]:

$$\theta_{UD} = \theta_{LD}\sqrt{1 - \frac{A}{3} - \frac{B}{6}};$$

here A and B are quadratic limb darkening coefficients and depend on the spectral type of the source[22]. For ζ Gem we used a limb darkening factor of $\theta_{UD}/\theta_{LD} = 0.963 \pm 0.006$ for all pulsational phases.

Table 1 Observations of ζ Gem made with the Palomar Testbed Interferometer between 3 March and 8 April 2000

Epoch (JD – 2,400,000.5)	Projected baseline (m)	Effective wavelength, λ_0 (μm)	V^2	θ_{UD} (mas)
51,605.226	103.60952	1.655	0.507 ± 0.012	1.679 ± 0.014
51,606.241	103.81611	1.646	0.502 ± 0.041	1.678 ± 0.046
51,607.280	103.94029	1.650	0.515 ± 0.050	1.651 ± 0.057
51,614.192	104.05741	1.651	0.450 ± 0.051	1.800 ± 0.059
51,615.180	104.83908	1.653	0.471 ± 0.027	1.740 ± 0.031
51,617.167	104.52214	1.653	0.539 ± 0.024	1.590 ± 0.028
51,618.143	106.38027	1.651	0.549 ± 0.006	1.538 ± 0.007
51,619.168	104.31558	1.653	0.557 ± 0.016	1.553 ± 0.018
51,620.169	104.14268	1.649	0.541 ± 0.024	1.589 ± 0.028
51,622.198	103.71849	1.651	0.498 ± 0.040	1.677 ± 0.046
51,643.161	103.56732	1.640	0.499 ± 0.010	1.666 ± 0.012

Each nightly observation consisted of 3–15 130-second integrations, interleaved with one calibration star and when possible one check star (see Table 2). Shown for each night is the mean epoch of observation, the mean projected baseline length, the SNR-weighted effective observing wavelength, the measured fringe visibility squared (V^2) and the best-fit uniform-disk diameter. For a circularly symmetric uniform intensity source the expected visibility is

$$V^2 = \left(\frac{2J_1(\pi B\theta_{UD}/\lambda_0)}{\pi B\theta_{UD}/\lambda_0}\right)^2$$

where J_1 is the first-order Bessel function, B is the projected aperture separation, θ_{UD} is the apparent angular diameter of the star in the uniform-disk model, and λ_0 is the centre-band wavelength of the observation. The uncertainties shown are statistical, derived from the internal scatter of the nightly measurements; the large variation in uncertainties between nights reflects variable atmospheric conditions as well as nightly variations in the amount of time spent observing the source.

curve[14] for ζ Gem. We then compared these radius changes to the interferometrically measured angular diameters, allowing us to solve for three unknown parameters: the mean radius of ζ Gem (R_ζ), the distance (d), and a phase shift ($\Delta\phi$). We include the phase shift because ζ Gem is known to be a somewhat imperfect pulsator with long-term changes in its periodicity[8]. The systematic uncertainties in the fit are from three sources. (1) The largest systematic effect is due to uncertainties in the diameter of the calibration star (Table 2). (2) A second source of systematic uncertainty comes from the fact that the observed spectrum is composed of emission from the entire disk while the radial velocity varies across the disk, being zero at the limbs. Thus we need a projection factor (p-factor) to relate the observed radial velocity to changes in the physical size of the star. We used a constant p-factor of 1.36 ± 0.05 appropriate for the published radial velocity data[15] with the uncertainty covering the range of plausible values. (3) Finally, there are uncertainties in the limb-darkening factors relating visibility to angular diameter.

All of the above uncertainties were propagated in the fit, resulting in separate statistical and systematic uncertainties. A fit of this model is shown in Fig. 2. The best-fit model parameters are: $d = 336 \pm 44\,(29/33)$ pc, $R_\zeta = 62 \pm 11\,(5/10)R_\odot$, where $R_\odot$ is the radius of the Sun, $\Delta\phi = 0.0054 \pm 0.018\,(0.018.0.0006)$ cycles, consistent with zero. Errors are given as $\sigma_{\rm total}(\sigma_{\rm statistical}/\sigma_{\rm systematic})$ with $\sigma^2_{\rm total} = \sigma^2_{\rm statistical} + \sigma^2_{\rm systematic}$. We obtained $\chi^2 = 10.0$ for 8 degrees of freedom (d.f.). We also fitted the model using uniform data weighting; the results changed by less than 1σ.

The resulting angular diameter and distance determination of ζ Gem is consistent with previous direct (but limited) measurements. Lunar occultation experiments[16] have found $\theta_{\rm UD} = 1.81 \pm 0.31$ mas at phase $\phi = 0.5961$; our best fit gives $\theta_{\rm UD} = 1.6 \pm 0.3$ at the same phase. Our distance determination is consistent that of ref. 10, that is, a distance to ζ Gem of 358 ± 113 pc. Observations of ζ Gem have also been made using the Navy Prototype Optical Interferometer (NPOI)[7]; these observations found a limb-darkened diameter, averaged over four epochs of observation, of 1.55 ± 0.09 mas, but did not detect pulsations. Using our best-fit parameters we have estimated the angular diameter at the same four epochs and obtain a mean limb-darkened diameter of 1.62 ± 0.3 mas (including systematic uncertainties)—in agreement with the NPOI measurement.

We note that further improvement in measurement accuracy is possible. At present the largest source of systematic uncertainty comes from the uncertainty in the angular diameter of the calibrator stars (Table 2). This uncertainty is most easily reduced by using multiple calibrators, particularly unresolved main-sequence stars. We plan future observations to reduce this uncertainty and hope to achieve 5% accuracy.

At the present level of accuracy, our results of distance and diameter are in excellent agreement with previously published results[17,18] based on application of the BW method and multicolour photometry which yield 410 ± 75 pc and a radius of $65R_\odot$. With continuing observations, interferometry will be in a position to either empirically validate the indirect methods or identify discrepancies and thus motivate improvements in theoretical modelling. In this context, it is worth noting that our second largest source of systematic uncertainty (a factor of about 3 smaller than the uncertainty due to the diameter of the calibrator stars, discussed above) comes from uncertainties in the theoretical modelling (such as the limb-darkening and the p-factor).

Whereas we can observe only half a dozen targets with the 100-m baseline PTI, a much larger number of Cepheids are accessible to longer baseline interferometers such as NPOI and CHARA[19]. Thus we anticipate that over the next few years distances to several dozen Cepheids will be determined with an accuracy of a few per cent, providing a direct calibration of the Cepheid period–luminosity relation. □

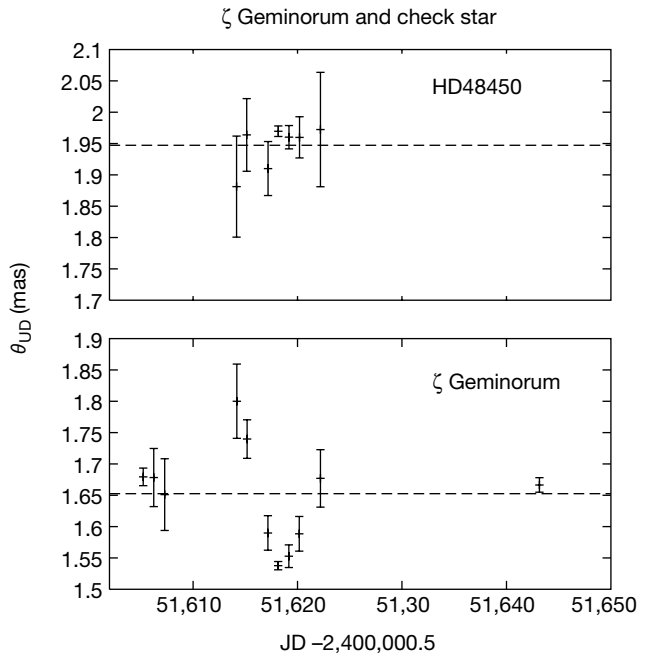

Figure 1 The uniform-disk (UD) angular diameter of ζ Gem as measured by PTI. Also shown is the UD angular diameter of the check star, HD48450. The dashed line is the unweighted mean of the data. The check star is well fitted by a constant diameter model (HD48450: $\theta_{\rm UD} = 1.965 \pm 0.006$ mas, $\chi^2_{\rm d.f.} = 0.5$). This value is consistent with the expected diameter. However, ζ Gem is not well fitted by a constant diameter model ($\chi^2_{\rm d.f.} = 19.7$). We argue (see text) that changes in the angular diameter of ζ Gem are due to pulsations and in Fig. 2 we present a fit to a pulsation model.

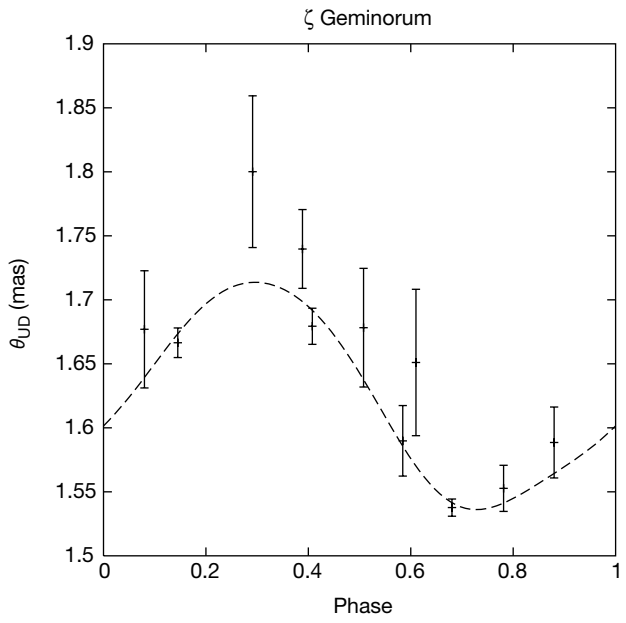

Figure 2 The UD angular diameter of ζ Gem as a function of pulsational phase with a model based on radial velocity data. Data is fitted for distance, mean radius and phase shift (see text). We assumed the period to be fixed at $P = 10.149244$ days during the time of observations, and calculated the phase shift with respect to the epoch JD 2,451,611.14505. The mean UD diameter is 1.653 mas and the real diameter is thus $1.653/0.963 = 1.717$ mas (see text and Table 2). At our inferred distance of 336 ± 44 pc we find the physical radius to be $62 \pm 11\ R_\odot$.

Received 22 June; accepted 21 July 2000.

1. Mould, J. R. *et al.* The Hubble Space Telescope key project on the extragalactic distance scale. XXVIII. Combining the constraints on the Hubble constant. *Astrophys. J.* **529,** 786–794 (2000).
2. Wesselink, A. J. Surface brightnesses in the U, B, V system with applications of M_V and dimensions of stars. *Mon. Not. R. Astron. Soc.* **144,** 297–311 (1969).
3. Krockenberger, M., Sasselov, D. D. & Noyes, R. W. Radii and distances of Cepheids. I. Method and measurement errors. *Astrophys. J.* **479,** 875–885 (1997).
4. Tanvir, N. R. in *Post-Hipparcos Cosmic Candles* 17–35 (Kluwer, Dordrecht, 1999).
5. Mourard, D. *et al.* The mean angular diameter of δ Cephei measured by optical long-baseline interferometry. *Astron. Astrophys.* **317,** 789–792 (1997).
6. Kervella, P. *et al.* in *Working on the Fringe: Optical and IR Interferometry from Ground and Space* 22–27 (ASP Conf. Ser. 194, Astronomical Society of the Pacific, San Francisco, 1999).
7. Nordgren, T. *et al.* Astrophysical quantities of Cepheid variables measured with the NPOI. (in the press).
8. Szabados, L. Northern Cepheids: Period update and duplicity effects. *Commun. Konkoly Observatory, Hungary* **96,** 123–244 (1991).
9. Laney, C. D. & Stobie, R. S. The radii of galactic Cepheids. *Mon. Not. R. Astron. Soc.* **274,** 337–360 (1995).
10. Perryman, M. A. C. *et al.* The HIPPARCOS Catalogue. *Astron. Astrophys.* **323,** L49–L52 (1997).
11. Colavita, M. M. *et al.* The Palomar Testbed Interferometer. *Astrophys. J.* **510,** 505–521 (1999).
12. Colavita, M. M. Fringe visibility estimators for the Palomar Testbed Interferometer. *Publ. Astron. Soc. Pacif.* **111,** 111–117 (1999).
13. Boden, A. F. *et al.* An interferometric search for bright companions to 51 Pegasi. *Astrophys. J.* **504,** L39–L42 (1998).
14. Bersier, D., Burki, G., Mayor, M. & Duquennoy, A. Fundamental parameters of Cepheids. II. Radial velocity data. *Astron. Astrophys.* **108,** 25–39 (1994).
15. Hindsley, R. & Bell, R. A. An investigation of photoelectric radial-velocity spectrometers as used in the analysis of Cepheid variables. *Publ. Astron. Soc. Pacif.* **98,** 881–888 (1986).
16. Ridgway, S. T. *et al.* Angular diameters by the lunar occultation technique. IV—Alpha Leo and the Cepheid Zeta Gem. *Astron. J.* **87,** 680–684 (1982).
17. Gieren, W. P., Barnes, T. G. & Moffett, T. J. The period-radius relation for classical Cepheids from the visual surface brightness technique. *Astrophys. J.* **342,** 467–475 (1989).
18. Gieren, W. P., Barnes, T. G. & Moffett, T. J. The Cepheid period-luminosity relation from independent distances of 100 galactic variables. *Astrophys. J.* **418,** 135–146 (1993).
19. McAlister, H. A. *et al.* Progress on the CHARA array. *Proc. SPIE* **3350,** 947–950 (1998).
20. Cohen, M. *et al.* Spectral irradiance calibration in the infrared. X. A self-consistent radiometric all-sky network of absolutely calibrated stellar spectra. *Astron. J.* **117,** 1864–1889 (1999).
21. Welch, D. L. Near-infrared variant of the Barnes-Evans method for finding Cepheid distances calibrated with high-precision angular diameters. *Astron. J.* **108,** 1421–1426 (1999).
22. Claret, A., Diaz-Cordoves, J. & Gimenez, A. Linear and non-linear limb-darkening coefficients for the photometric bands R I J H K. *Astron. Astrophys.* **114,** 247–252 (1995).

Acknowledgements

We thank R. Akeson, T. Armstrong, A. Bouchez, M. Colavita, T. Nordgren, M. Nunez and D. Sasselov for valuable comments. Part of the work described in this paper was performed at the Jet Propulsion Laboratory under contract with the National Aeronautics and Space Administration. This research has made use of the Simbad database, operated at Centre de Données astronomiques de Strasbourg, Strasbourg, France. B.F.L. gratefully acknowledges the support of NASA through the Michelson fellowship programme. B.F.L. acknowledges the support of NASA and the NSF.

Correspondence and requests for materials should be addressed to B.F.L. (e-mail: bfl@astro.caltech.edu).

Simulating dynamical features of escape panic

Dirk Helbing*†, Illés Farkas‡ & Tamás Vicsek*‡

* *Collegium Budapest–Institute for Advanced Study, Szentháromság u. 2, H-1014 Budapest, Hungary*
† *Institute for Economics and Traffic, Dresden University of Technology, D-01062 Dresden, Germany*
‡ *Department of Biological Physics, Eötvös University, Pázmány Péter Sétány 1A, H-1117 Budapest, Hungary*

One of the most disastrous forms of collective human behaviour is the kind of crowd stampede induced by panic, often leading to fatalities as people are crushed or trampled. Sometimes this behaviour is triggered in life-threatening situations such as fires in crowded buildings[1,2]; at other times, stampedes can arise during the rush for seats[3,4] or seemingly without cause. Although engineers are finding ways to alleviate the scale of such disasters, their frequency seems to be increasing with the number and size of mass events[2,5]. But systematic studies of panic behaviour[6–9] and quantitative theories capable of predicting such crowd dynamics[5,10–12] are rare. Here we use a model of pedestrian behaviour to investigate the mechanisms of (and preconditions for) panic and jamming by uncoordinated motion in crowds. Our simulations suggest practical ways to prevent dangerous crowd pressures. Moreover, we find an optimal strategy for escape from a smoke-filled room, involving a mixture of individualistic behaviour and collective 'herding' instinct.

Up to now, panic as a particular form of collective behaviour occurring in situations of scarce or dwindling resources[1,6] has been mainly studied from the perspective of social psychology[7–9]. Panicking individuals tend to show maladaptive and relentless mass behaviour like jamming and life-threatening overcrowding[1–4,8], which has often been attributed to social contagion[1,4,8] (see ref. 9 for an overview of theories). The observed jamming is a result of uncoordinated motion ('incoordination') and depends on the reward structure[6].

We have studied related socio-psychological literature[6–9], reports in the media and available video materials (see http://angel.elte.hu/~panic/), empirical investigations[1–3], and engineering handbooks[13,14]. The characteristic features of escape panics can be summarized as follows: (1) People move or try to move considerably faster than normal[13]. (2) Individuals start pushing, and interactions among people become physical in nature. (3) Moving and, in particular, passing of a bottleneck becomes uncoordinated[6]. (4) At exits, arching and clogging are observed[13]. (5) Jams build up[7]. (6) The physical interactions in the jammed crowd add up and cause dangerous pressures up to 4,450 N m^{-1} (refs 2, 5) which can bend steel barriers or push down brick walls. (7) Escape is further slowed by fallen or injured people acting as 'obstacles'. (8) People show a tendency towards mass behaviour, that is, to do what other people do[1,8]. (9) Alternative exits are often overlooked or not efficiently used in escape situations[1,2].

These observations have encouraged us to model the collective phenomenon of escape panic in the framework of self-driven many-particle systems. Our computer simulations of the crowd dynamics of pedestrians are based on a generalized force model[15], which is particularly suited to describing the fatal build up of pressure observed during panics[2–5]. We assume a mixture of socio-psychological[16] and physical forces influencing the behaviour in a crowd: each of N pedestrians i of mass m_i likes to move with a certain desired speed v_i^0 in a certain direction $\mathbf{e}_i^0$, and therefore tends to correspondingly adapt his or her actual velocity $\mathbf{v}_i$ with a certain characteristic time τ_i. Simultaneously, he or she tries to keep a velocity-dependent distance from other pedestrians j and walls W. This can be modelled by 'interaction forces' $\mathbf{f}_{ij}$ and $\mathbf{f}_{iW}$, respectively. In mathematical terms, the change of velocity in time t is then given by the acceleration equation

$$m_i \frac{\mathrm{d}\mathbf{v}_i}{\mathrm{d}t} = m_i \frac{v_i^0(t)\mathbf{e}_i^0(t) - \mathbf{v}_i(t)}{\tau_i} + \sum_{j(\neq i)} \mathbf{f}_{ij} + \sum_W \mathbf{f}_{iW} \qquad (1)$$

while the change of position $\mathbf{r}_i(t)$ is given by the velocity $\mathbf{v}_i(t) = \mathrm{d}\mathbf{r}_i/\mathrm{d}t$. We describe the psychological tendency of two pedestrians i and j to stay away from each other by a repulsive interaction force $A_i \exp[(r_{ij} - d_{ij})/B_i]\mathbf{n}_{ij}$, where A_i and B_i are constants. $d_{ij} = ||\mathbf{r}_i - \mathbf{r}_j||$ denotes the distance between the pedestrians' centres of mass, and $\mathbf{n}_{ij} = (n_{ij}^1, n_{ij}^2) = (\mathbf{r}_i - \mathbf{r}_j)/d_{ij}$ is the normalized vector pointing from pedestrian j to i. The pedestrians touch each other if their distance d_{ij} is smaller than the sum $r_{ij} = (r_i + r_j)$ of their radii r_i and r_j. In this case, we assume two additional forces inspired by granular interactions[17,18], which are essential for understanding the particular effects in panicking crowds: a 'body force' $k(r_{ij} - d_{ij})\mathbf{n}_{ij}$ counteracting body compression and a 'sliding friction force' $\kappa(r_{ij} - d_{ij})\Delta v_{ji}^t \mathbf{t}_{ij}$ impeding relative tangential motion, if pedes-